

## CHAPTER 5. NUMERICAL MODELING OF CONCRETE CURING

Concrete curing involves complex interactions of numerous variables. The numerical model in this section varies thermal conductivity, tension strength, modulus, heat generation, hydration phases, and volume expansion. Resulting compression stresses, cracking, and temperature are computed, which in turn affect the material properties and chemical reactions.

The following study compares a drilled shaft surrounded by rock to a drilled shaft surrounded by clay. All other factors are identical. The surrounding ground temperature is set to 10° C. The concrete is initially placed at 45° C. A very warm concrete temperature is used to encourage cracking. The first five days of concrete curing is simulated. This is sufficient time due to the high temperatures and high rates of hydration caused by the high initial concrete temperature. High placement temperatures are not recommended, as this study will show.

Rock and clay have different thermal conductivities, but the thermal effects on cracking are less pronounced in this scenario. A lower initial concrete temperature would show sharper differences in curing rates, cracking, and internal stress due to differences in thermal conductivity of the surrounding environment. For this reason, chemical modeling should be seriously considered to study complex interactions of variables for various scenarios, beyond the case presented in this study.

### 5.1 Empirical Curing Model Method

Figure 5.1 plots the heat of hydration curves used in the model. These curves can be obtained empirically for a particular concrete mix by measuring heat generation under isothermal conditions.

Table 5.1 lists the actual coefficients used in the model. The high temperature curve in Figure 5.1 corresponds to 50° C in the table. The average temperature corresponds to 30° C, and the low temperature corresponds to 10° C. All the curves have a rapid initial hydration phase that quickly completes within the first few minutes of concrete placement, depending on the temperature of the concrete. According to Table 5.1, the first hydration phase releases heat during first half hour at a concrete temperature of 10° C, but generates the same heat in the first 12 minutes at a higher temperature of 50° C. The curves in Figure 5.1 produce the same heat at different rates, depending on the concrete temperature, assuming that all the cement hydrates according to the same chemical reactions. This is not always the case, and should be validated empirically by isothermal lab tests. The shape of the curves corresponds to the different hydration reactions that concrete typically undergoes throughout the curing process.

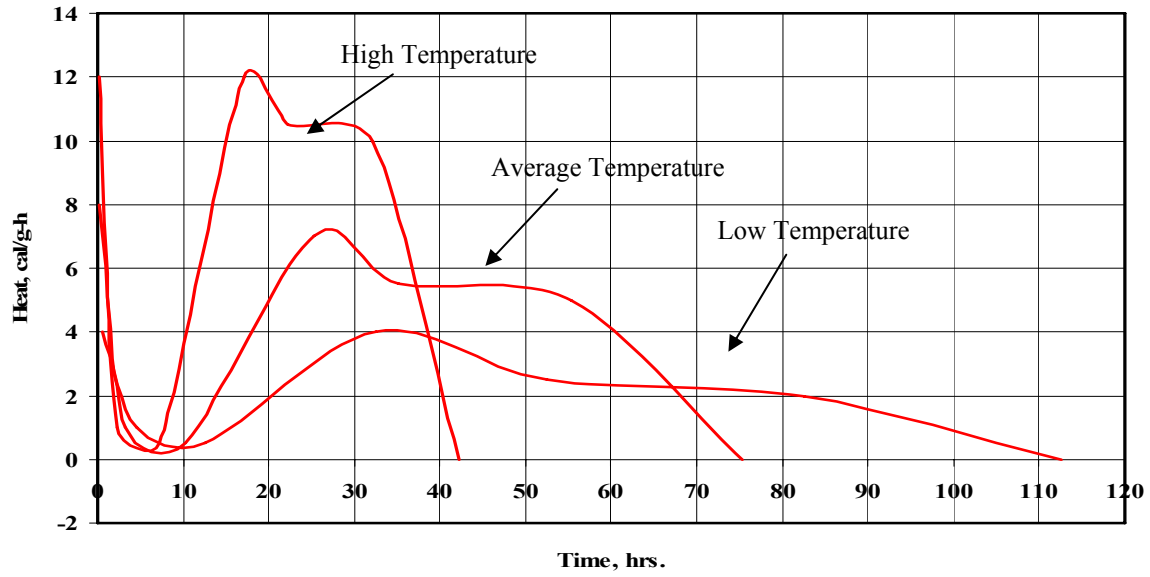


**Figure 5.1. Chart. Rate of Heat Generation (Cal/hr) used in the Numerical Mode**

The concrete curing model interpolates model parameters from Table 5.1 depending on the concrete temperature and hydration phase for each concrete particle element in the model. The rate of change of the hydration phase is also interpolated from the table, and updated for each concrete element. Thermal conductivity, strength, modulus, and particle volume are updated in a similar fashion. This allows the model to simulate complex interactions of parameters at a fundamental level, using empirical values tabulated from straightforward lab tests.

**Table 5.1 Curing Model Coefficients**

Temperature (C)	Hydration %	Heat	Time (hrs)	Thermal Conductivity	Strength	Stiffness	Radius
10	0	4	0.5	0.25	0.25	0.25	1
10	17	1	4	0.3	0.5	0.5	0.99
10	33	0.5	8	0.35	0.6	0.6	0.98
10	50	4	20	0.4	0.7	0.7	0.97
10	67	2.5	20	0.45	0.8	0.8	0.96
10	83	2	30	0.5	0.9	0.9	0.95
10	100	0	30	0.55	1	1	0.94
30	0	8	0.25	0.25	0.25	0.25	1
30	17	1	3	0.3	0.5	0.5	0.99
30	33	0.5	7	0.35	0.6	0.6	0.98
30	50	7	15	0.4	0.7	0.7	0.97
30	67	5.5	10	0.45	0.8	0.8	0.96
30	83	5	20	0.5	0.9	0.9	0.95
30	100	0	20	0.55	1	1	0.94
50	0	12	0.2	0.25	0.25	0.25	1
50	17	1	2	0.3	0.5	0.5	0.99
50	33	0.5	5	0.35	0.6	0.6	0.98
50	50	12	10	0.4	0.7	0.7	0.97
50	67	10.5	5	0.45	0.8	0.8	0.96
50	83	10	10	0.5	0.9	0.9	0.95
50	100	0	10	0.55	1	1	0.94

## 5.2 Curing Model Presentation

The following figures display various properties at different stages in the concrete curing process. All the figures show the drilled shaft in rock on the left, the drilled shaft in clay in the center, and the difference on the right. Many of the difference scales have been amplified for display purposes. See section 6.1 for details on the color schemes, property scales, and model parameters used in this simulation.

Certain properties are displayed for discussion purposes, but are not exhaustive. Compression, fracture extent, heat generation, hydration phase, and temperature are shown, while other properties such as material tensile strength, modulus, and thermal conductivity are not shown. Changes in element volume and displacement are shown indirectly.

Figures 5.2 - 5.5 show the compression effects of concrete curing. The compression is defined as the average force exerted on an element by attached springs. A zero compression value does not mean the element is not under compression, but that the sum of all compression and tension forces averages to zero. Initial compression was set to zero to show the effects of concrete curing. This is a reasonable assumption, since shaft excavation relieves lateral compression in clay.

Figures 5.6 - 5.9 show the fracture extent. Initially, no cracks are introduced in the concrete. This is a valid assumption, as concrete slowly changes from a fluid to a solid state. The surrounding clay is randomly initialized with 5% cracking, to simulate more realistic conditions. Each element color is determined from the number of non-broken springs attached to the element. This scheme has the effect of magnifying crack severity for display purposes, and should be taken into account when interpreting the images. A single broken spring will affect the display of two elements. Crack propagation can be traced by comparing images at different times.

Figures 5.10 - 5.13 show the heat of hydration generated from the chemical reactions. Each concrete element in the model will release basically the same amount of heat during the curing process, but potentially at different rates, depending on the temperature of the concrete. The temperature is a function of heat generation and heat transfer over time, which in turn may be affected by cracking and shrinkage of the concrete, and deconsolidation of the clay. It is important to keep in mind the many complex interactions are involved in the modeling.

Figures 5.14 - 5.17 show the hydration phase of each concrete element in the model, as a percentage of completion. Other properties, such as thermal conductivity, modulus, strength, and shrinkage often are closely correlated to the hydration phase. As the concrete changes chemical composition, the material properties of the concrete are affected correspondingly. For this reason, material properties such as thermal conductivity, modulus, strength, and shrinkage are not included in the plots.

Figures 5.18 - 5.21 show the resulting temperature of each element in the model, generated from the chemical reactions and transferred by conduction and convection. Conduction is modeled in a traditional fashion, depending on contact and thermal conductivity coefficients. Convection is modeled by retaining spring connections after fracture. Heat is allowed to transfer across springs that are broken, at a reduced rate, depending on the separation. Spring connections greater than two times the element radius are eliminated, so convection is not modeled across large crack separation. Radiation was not considered a significant factor in this study, so was not modeled.

### **5.3 Curing Model Simulation**

The following discussion may require observation of several figures at once, due to complex interaction of various parameters during the curing phase. To minimize confusion, each parameter will be discussed individually throughout the curing process.

#### **5.3.1 Compression**

The top row of Figure 5.2 shows the compression after 4 hours. At this stage, the first hydration phase has completed, and the second hydration phase is in a very early stage.

The concrete has started to shrink slightly after the initial hydration phase. The top left image shows that the concrete is under relatively high tension at this stage, shown in magenta. This is because the concrete has not debonded from the rock, and has a very low modulus at this early stage. The rock shows no change in stress, because the rock has a much higher stiffness. The top center image shows that the clay surrounding the concrete starts to deconsolidate as the shaft shrinks. Clay has a much lower stiffness than rock, so tension forces allow more deformation in the clay. The cohesion forces and interlocking between the clay and the concrete are strong enough at this stage to cause deformation and deconsolidation of the clay, rather than debonding from the concrete. The entire shaft is still under tension, but the tension is less around the perimeter of the shaft, due to the deformation of the clay. This difference is more pronounced in the difference image at the top right. This shows that the tension in the center of the shaft is the same for both models, but slightly lower in the outer portions of the shaft around the rebar cage, due to the deformation in the clay.

The tension stress in the shaft is large enough to overcome cohesion forces bonding the rebar and access tubes to the concrete. This debonding affects the compression stresses in the shaft. Careful observation indicates that the tension forces are lower in regions near the rebar and access tubes. These lower tensions are a result of the different thermal expansion rates between steel and concrete, and also due to the differences in initial temperature and thermal conductivity. The steel was initialized at 10° C, while the concrete was placed at 45° C. The difference in temperature as heat transfers from the warm concrete to the cool steel results in a different hydration rate in the vicinity of the rebar, causing lower initial stiffness and lower initial strength in the adjacent concrete. These property changes result in lower tension in these regions, but because of the lower strength, slight debonding begins to occur even at this very early stage in the curing process. The debonding between steel and concrete is slightly more pronounced in the shaft surrounded by rock, because of the higher tension forces in the perimeter of the shaft.

After 8 hours, as shown in the bottom row of Figure 5.2, the second hydration phase is beginning to generate heat in warmer regions of the concrete. The concrete continues to shrink, expanding the region of clay deconsolidation, and reducing tension around the rebar. Tension in the concrete around the rebar in the shaft surrounded by rock has reached zero, in some regions. The difference plot shows much lower tension forces in the shaft surrounded by rock in regions around the rebar, but higher tension forces along the perimeter. The higher tension forces along the perimeter are due to the high stiffness of the rock.

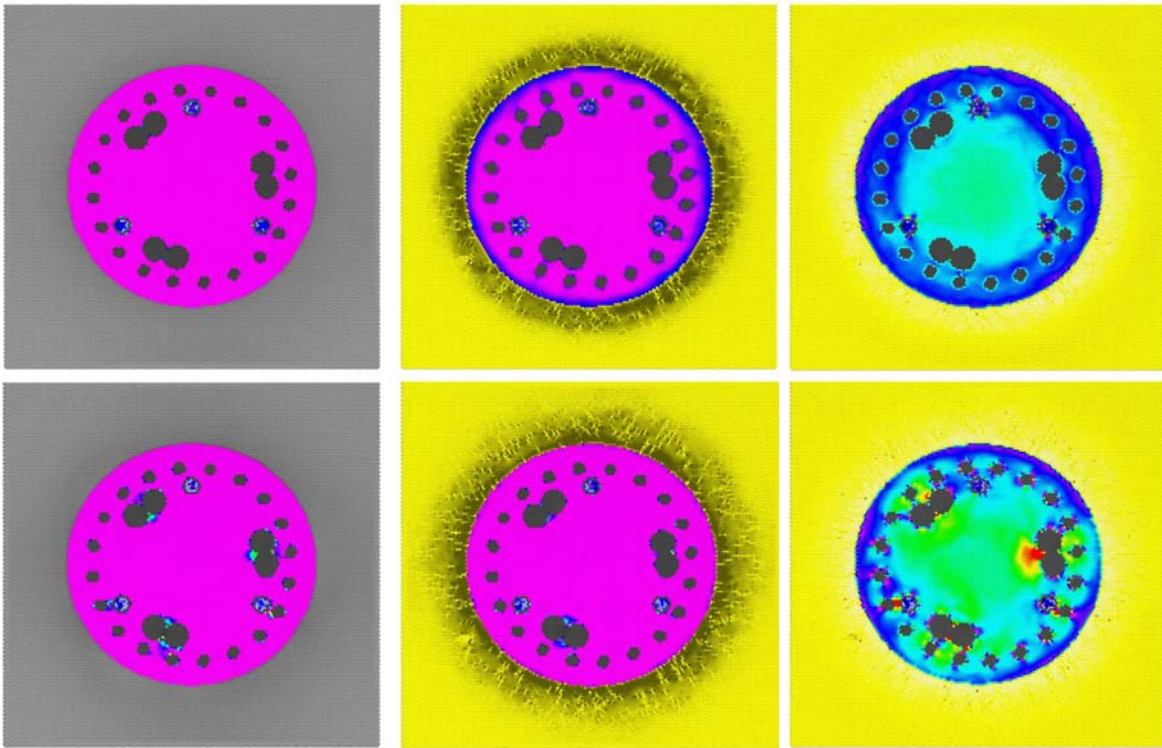


**Figure 5.2. Plot. Curing Compression. Top: 4 hours. Bottom: 8 hours. Left: Rock. Middle: Clay. Right: Difference**

The large differences in tension stress are a result of the stiffness of the surrounding ground, not due to differences in thermal conductivity. This is an important factor which is easily overlooked in the analysis of thermal cracking. This factor is more pronounced for higher concrete placement temperatures, but is still a major contributing factor in thermal cracking in other scenarios as well.

The top row of Figure 5.3 shows the compression stress condition at 12 hours, as more heat is generated from the second hydration phase. Careful observation of the image on the left shows a release in tension forces in the rock at the left of the shaft, as tension forces in the strengthening concrete begin to overcome the cohesion and interlocking forces bonding the concrete to the rock. Tension forces remain lower in the perimeter of the shaft surrounded by clay. The tension forces in the center of the shaft are basically the same for both cases.

The bottom row of Figure 5.3 shows the compression stress condition at 24 hours, at the peak of the second hydration phase. The shaft on the left exhibits a sharp decrease in tension forces along the perimeter of the shaft, after the concrete fully debonds from the surrounding rock. However, the high variations in compression in the vicinity of the rebar are a result of cracking,

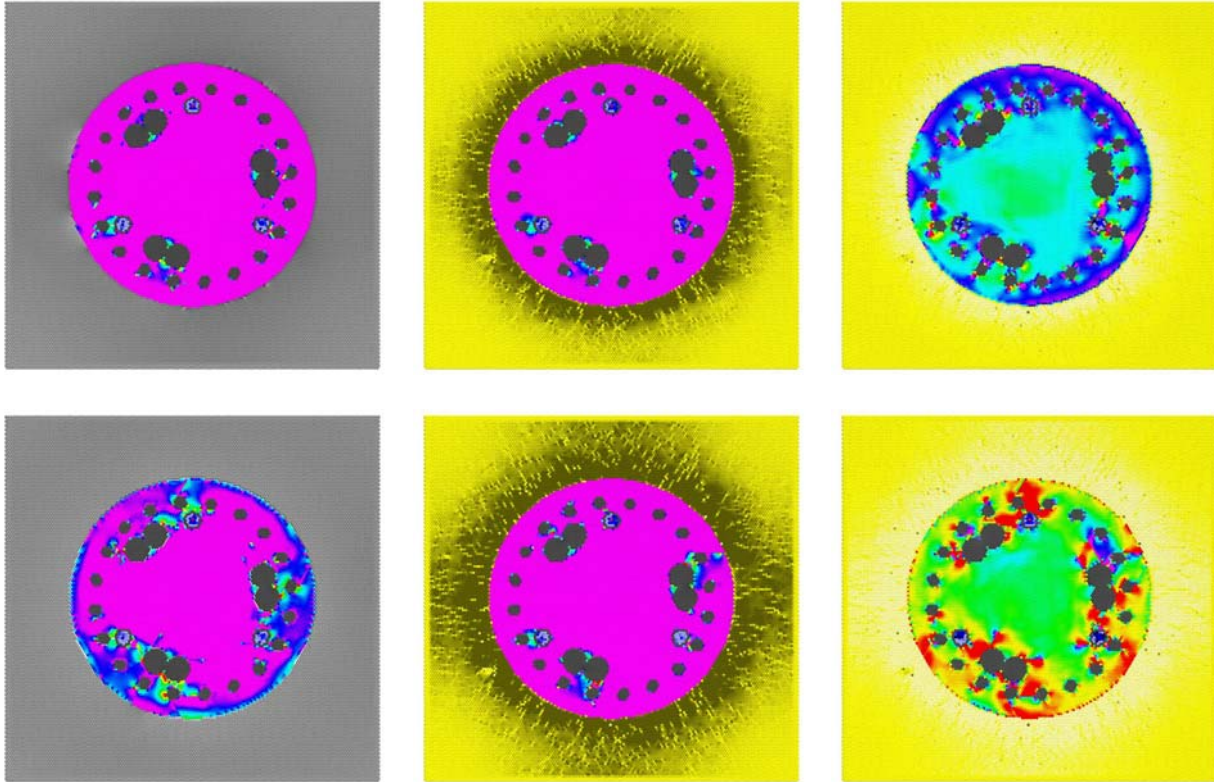


**Figure 5.3. Plot. Curing Compression. Top: 12 hours. Bottom: 24 hours. Left: Rock. Middle: Clay. Right: Difference**

due to the high tensile stresses formed before debonding with the rock. The clay has not debonded, so the clay continues to deconsolidate as the shaft shrinks.

The top row of Figure 5.4 shows the compression stress condition at 2 days, at the peak of the third hydration phase. Compression stress continues to build in the shaft on the left in the region of the rebar. The rock now has no effect on compression stress, except indirectly through convection cooling. Tension stresses in the clay have increased to the point of initiating slight debonding between the clay and the concrete. Debonding appears to occur first in the regions adjacent to the rebar. The compression stress does not clearly indicate why debonding occurs first in this region. However, internal compression stress has increased to positive levels for the first time in some regions. The compression stress has reached levels capable of deforming the access tubes.

The thickness of the access tube is only one element at this resolution, and is unable to provide the proper shear resistance force. The difference image on the right has some very interesting features. As micro-cracks propagate, regions of high stress concentrate at the point of the crack. Two of these regions can be seen near the center of the shaft. The bottom row of Figure 5.4 shows the compression stress condition at 3 days, at the end of the third hydration phase. Very little additional heat is generated after this point, but the shaft continues to cool, shrink, and

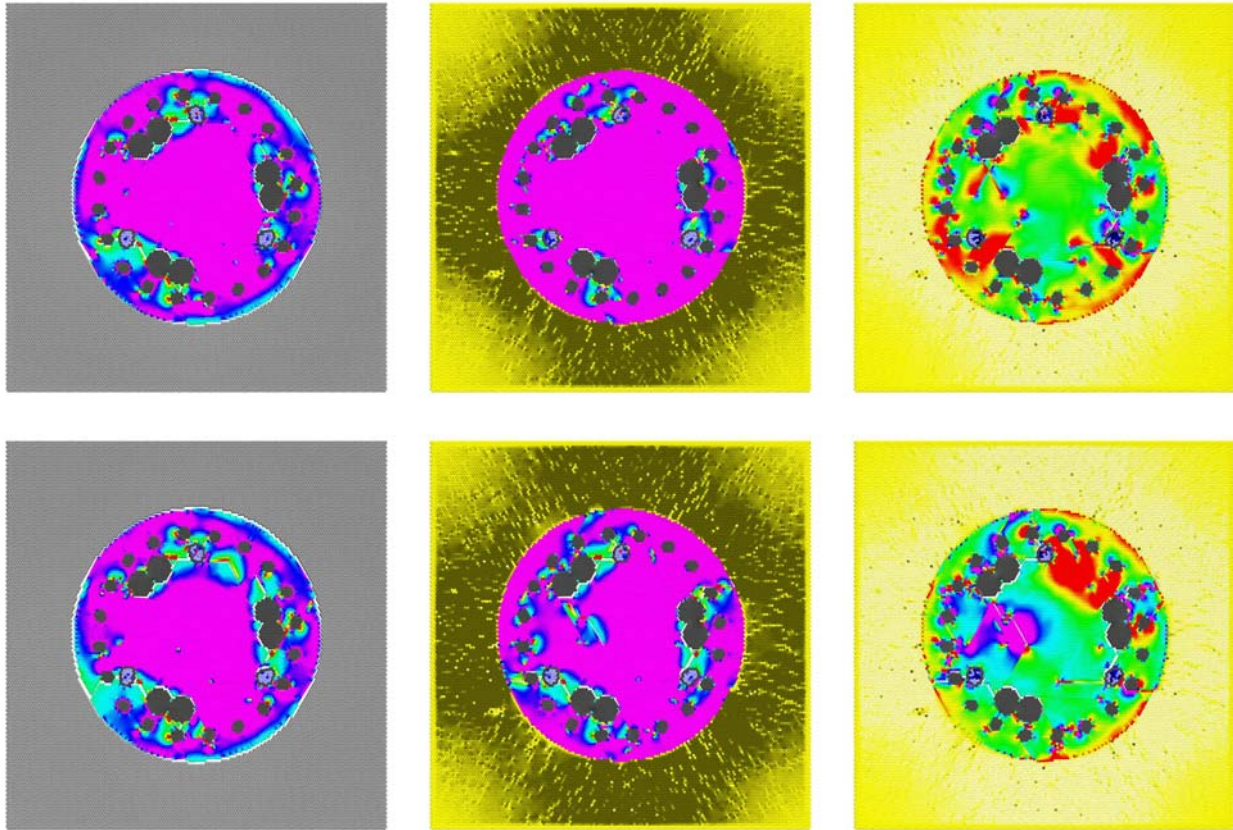


**Figure 5.4. Plot. Curing Compression. Top: 2 days. Bottom: 3 days. Left: Rock. Middle: Clay. Right: Difference**

crack. Compression stress at this stage is closely correlated to rebar and tube debonding, and internal cracking of the shaft.

After 4 days, the shaft compression stress has stabilized, as shown in Figure 5.5. The overall internal stress in the shaft surrounded by rock is nearly zero, but with pockets under high tension and compression. The high tension at the perimeter of the shaft is of concern, because of a higher future cracking potential that could weaken the shaft and expose the rebar to corrosives. The surrounding rock is unaffected, but the clay has deconsolidated to greater than one radius away from the shaft. This is a serious concern, because soil near the surface contributes significant support to the foundation. Reduction in the consolidation of the surrounding ground due to excavation and concrete shrinkage can lower the shaft capacity.

The internal stresses in the shaft surrounded by clay are more pronounced, especially in tension. These stresses will persist in the shaft, unless disrupted by additional cracking. Regions under tension are most likely to crack under future loading. Although both cases have similar fracture extent, the shaft surrounded by clay is much weaker, due to trapped pockets of internal tension.

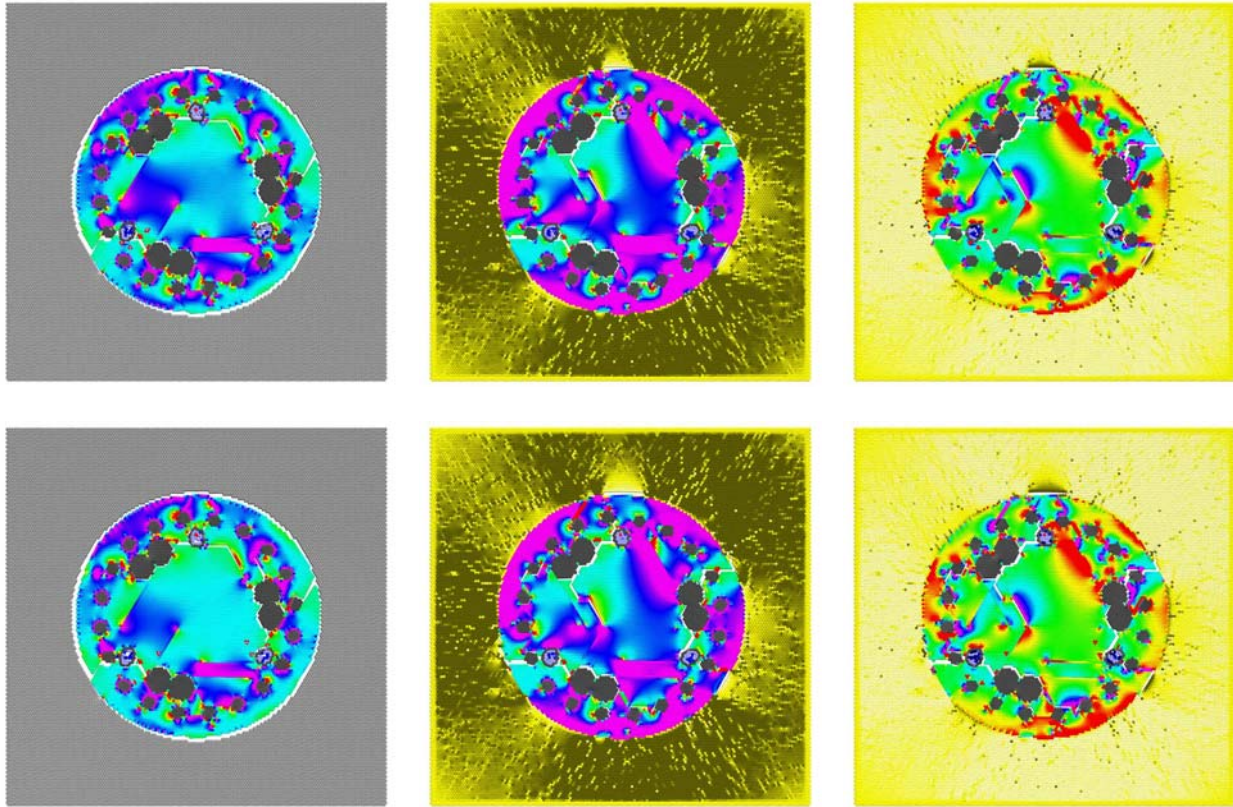


**Figure 5.5. Plot. Curing Compression. Top: 4 days. Bottom: 5 days. Left: Rock. Middle: Clay. Right: Difference**

### 5.3.2 Cracking

The top row of Figure 5.6 shows the cracking extent 4 hours after concrete placement. Slight cracking can be observed around access tubes. Although debonding occurs at an early stage, NDE techniques such as CSL can only detect debonding at later stages after significant separation. The bottom row of Figure 5.6 shows the cracking extent 8 hours after concrete placement, between the first and second hydration phases. At this stage, micro-cracks have formed in the concrete completely around all access tubes and rebar in the shaft surrounded by rock. The higher tension forces pull the concrete away from the steel, breaking the weak cohesive bonds. Due to cooler temperatures surrounding the steel, the concrete in these regions is not as mature as concrete in warmer portions of the shaft. The shaft surrounded by clay shows more debonding around the large rebar. The higher thermal conductivity and greater volume of the rebar has the effect of reducing the temperature of adjacent concrete.

Lower temperatures slow hydration, which in turn delay development of concrete strength and stiffness. Narrow regions of concrete between closely spaced rebar, and between rebar adjacent to access tubes, begins to crack at this stage.

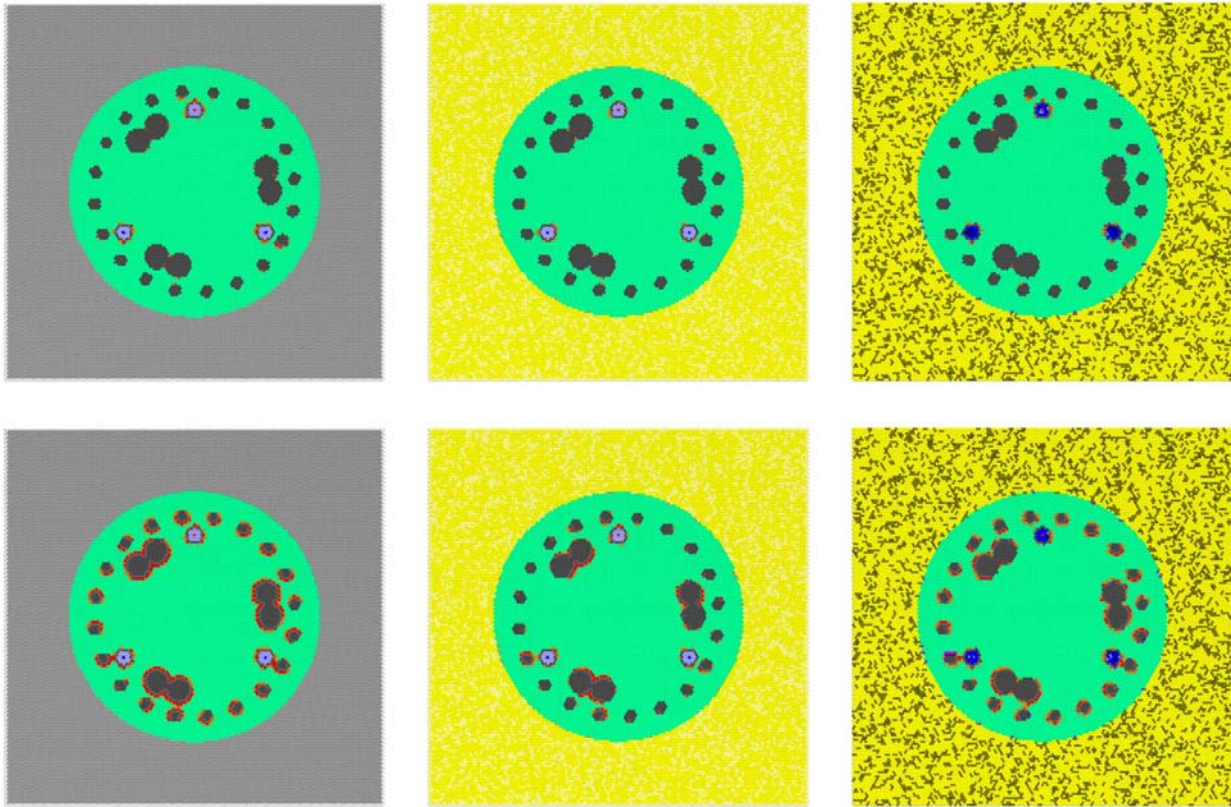


**Figure 5.6. Plot. Curing Fracture. Top: 4 hours. Bottom: 8 hours. Left: Rock. Middle: Clay. Right: Difference**

The top row of Figure 5.7 shows the fracture extent at 12 hours, as more heat is generated from the second hydration phase. Early stages of debonding can be detected between the concrete and the surrounding rock. The lower clay stiffness results in higher displacements, allowing the clay to deconsolidate before debonding from the shaft. Internally, cracks begin to propagate from the rebar in the shaft surrounded by rock, generally parallel to the perimeter of the shaft where tension forces are greatest. A small crack can be seen extending from the rebar toward the debonded rock in the lower left of the image. It is interesting to note that thermal cracking propagates from the inside of the shaft out, and initiates at the rebar.

The bottom row of Figure 5.7 shows the fracture extent at 24 hours, at the peak of the second hydration phase. Cracks surrounding the shaft on the left indicate complete debonding between the concrete and surrounding rock. More cracks have formed along the perimeter of the shaft between the rebar and access tubes. Cracks have also developed from the rebar to the outside of the shaft.

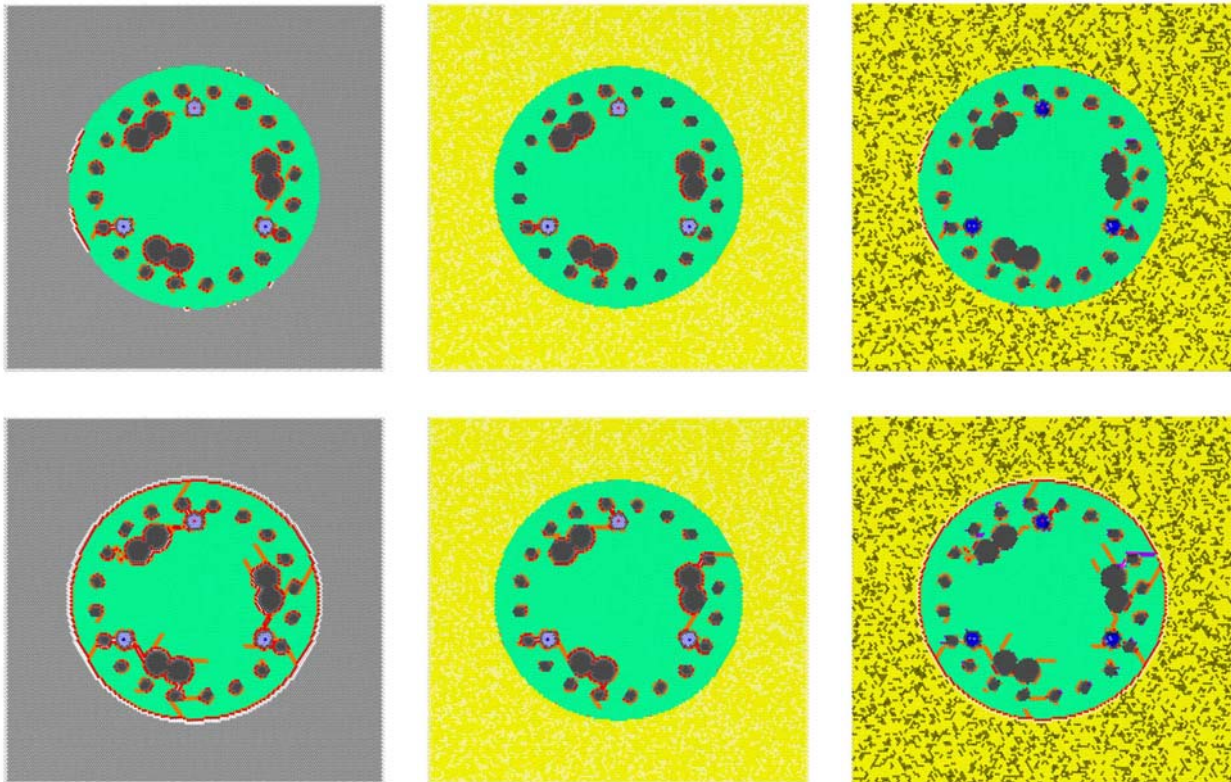


**Figure 5.7. Plot. Curing Fracture. Top: 12 hours. Bottom: 24 hours. Left: Rock. Middle: Clay. Right: Difference**

The top row of Figure 5.8 shows cracking extent at 2 days, at the peak of the third hydration phase. Cracks in both cases have extended almost entirely around the shaft in the region of the rebar cage. Cracks in the shaft surrounded by clay also extend across the central regions of the shaft.

The bottom row of Figure 5.8 shows cracking extent at 3 days, at the end of the third hydration phase. No additional cracking is observed, indicating that cracking has stabilized after 2 days. Figure 5.9 verifies this stabilization, as no change in cracking is observed after day 4.

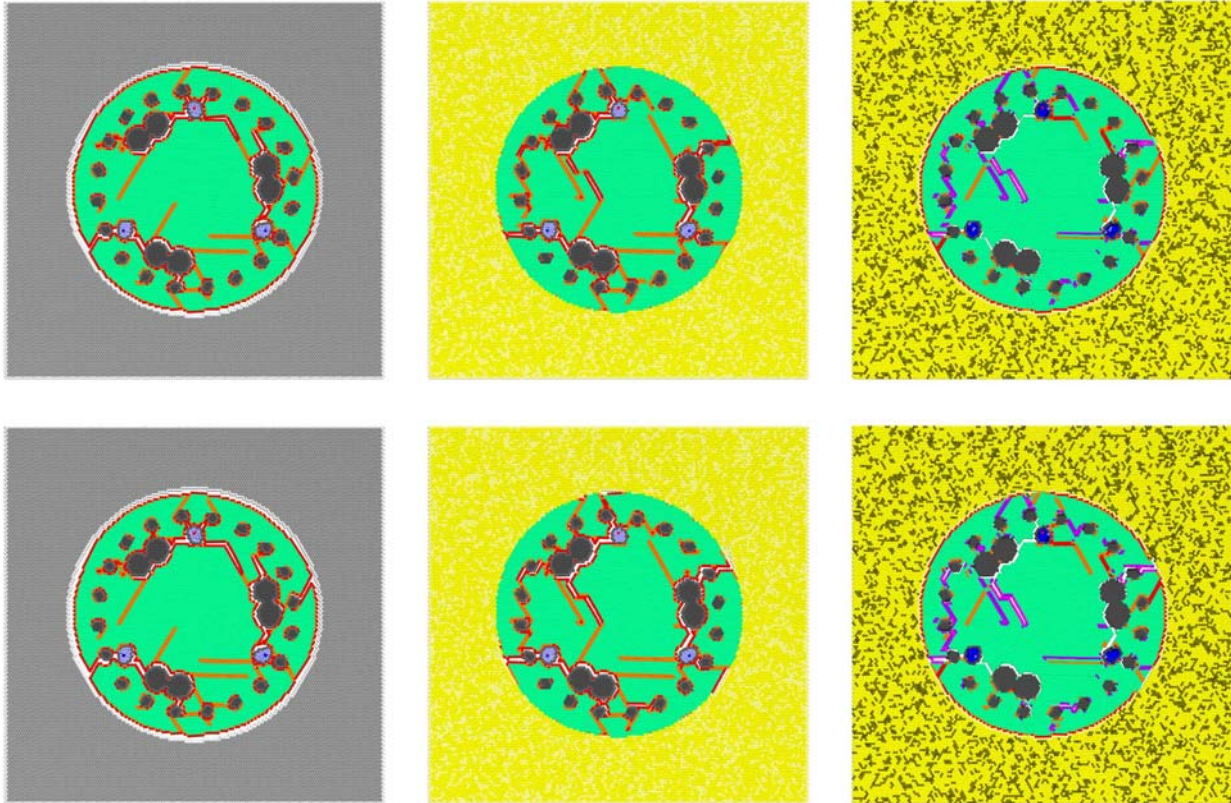


**Figure 5.8. Plot. Curing Fracture. Top: 2 days. Bottom: 3 days. Left: Rock. Middle: Clay. Right: Difference**

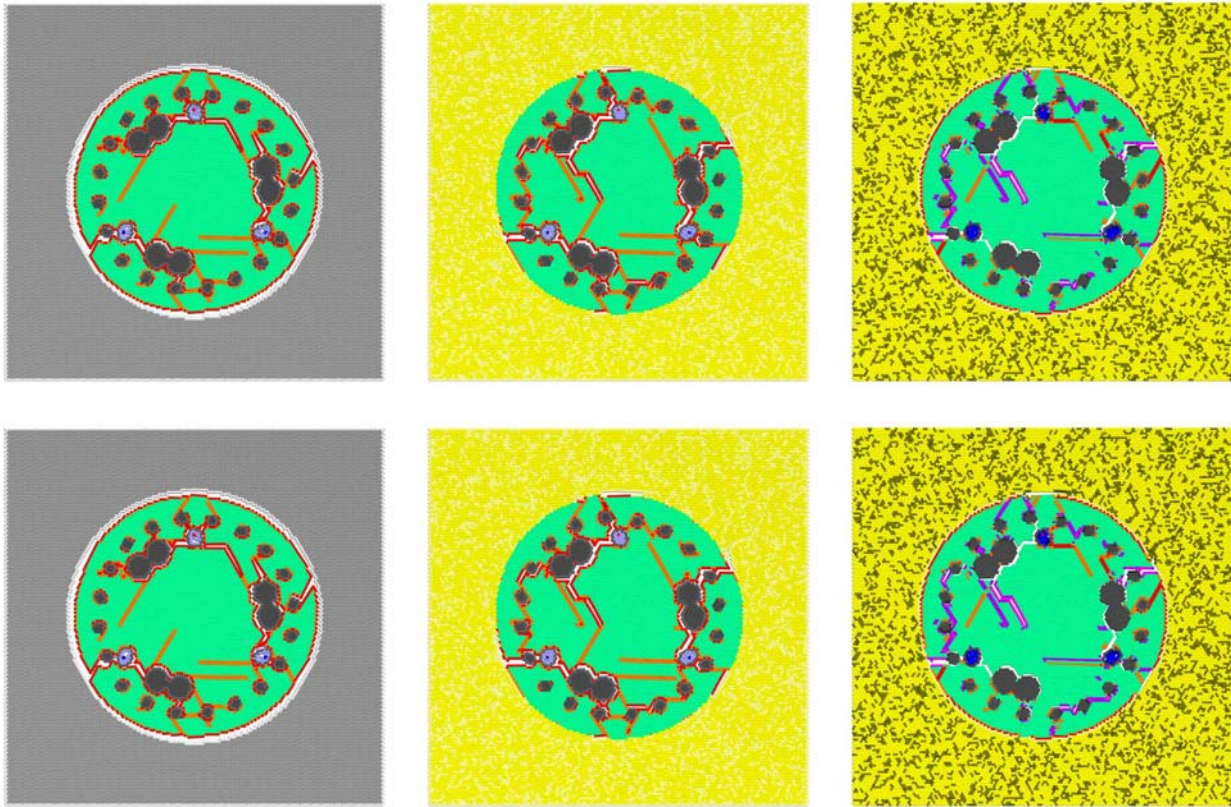


**Figure 5.9. Plot. Curing Fracture. Top: 4 days. Bottom: 5 days. Left: Rock. Middle: Clay. Right: Difference**

### 5.3.3 Heat

The top row of Figure 5.10 shows the heat generated from hydration 4 hours after concrete placement. This is the stage between the first and second hydration phases, so no heat is generated in either case.

The bottom row of Figure 5.10 shows the heat generated from hydration 8 hours after concrete placement. Most of the concrete is in early stages of the second hydration phase. Regions around the rebar and the perimeter of the shaft have cooler temperatures due to heat transfer, so this concrete has not yet entered the second hydration phase. The combination of cooler temperatures and delayed heat generation result in further delay of concrete curing in these regions. Less heat is generated in concrete adjacent to the clay because of the difference in thermal conductivity between the clay and the rock. Clay has higher thermal conductivity, so more heat is transferred into the surrounding clay than into the rock. These lower temperatures result in delayed hydration around the perimeter.

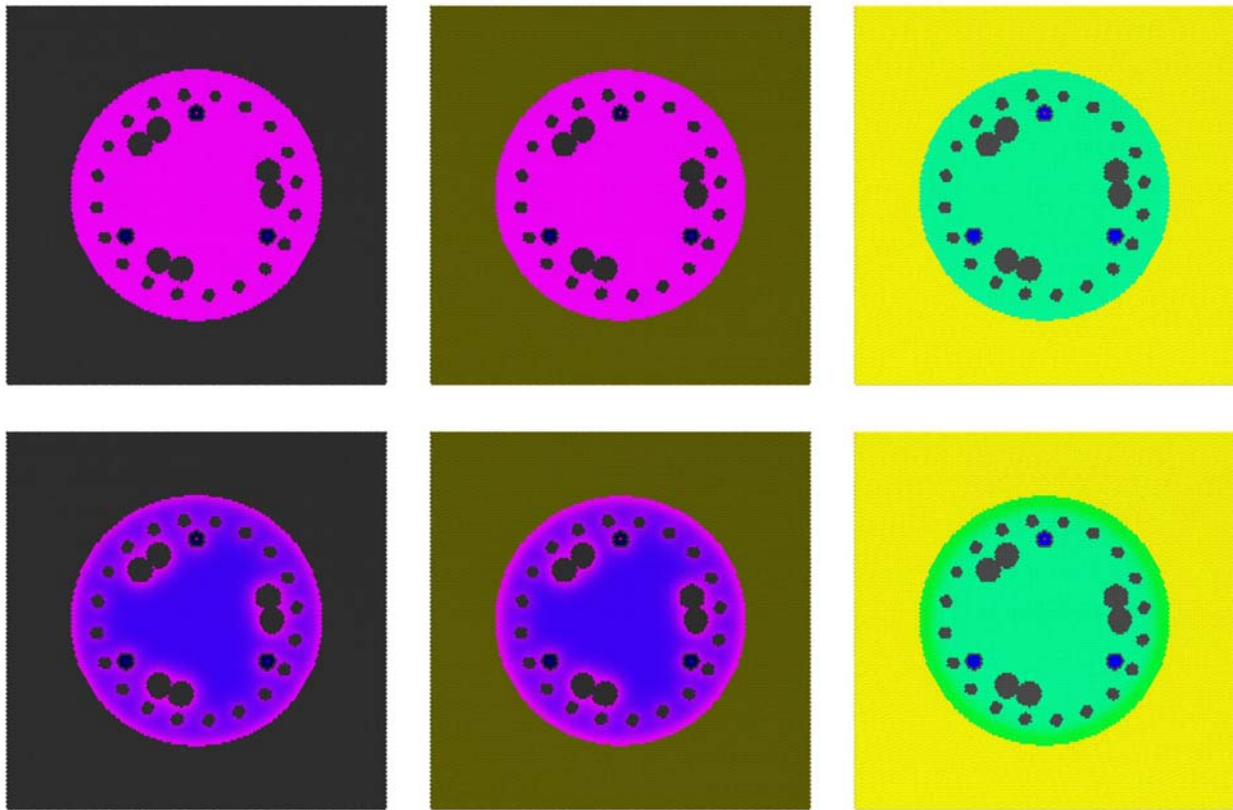


**Figure 5.10. Plot. Curing Heat. Top: 4 hours. Bottom: 8 hours. Left: Rock. Middle: Clay. Right: Difference**

The top row of Figure 5.11 shows the heat generated at 12 hours. The center of the shaft has reached the peak of the second hydration phase, due to the high placement temperature, and sustained high temperatures. Concrete in the region of the rebar, where temperatures are cooler, is at the beginning of the second hydration phase.

The bottom row of Figure 5.11 shows the heat generated at 24 hours. Heat generation is more uniform throughout the shaft, although the concrete is not at the same maturity level.

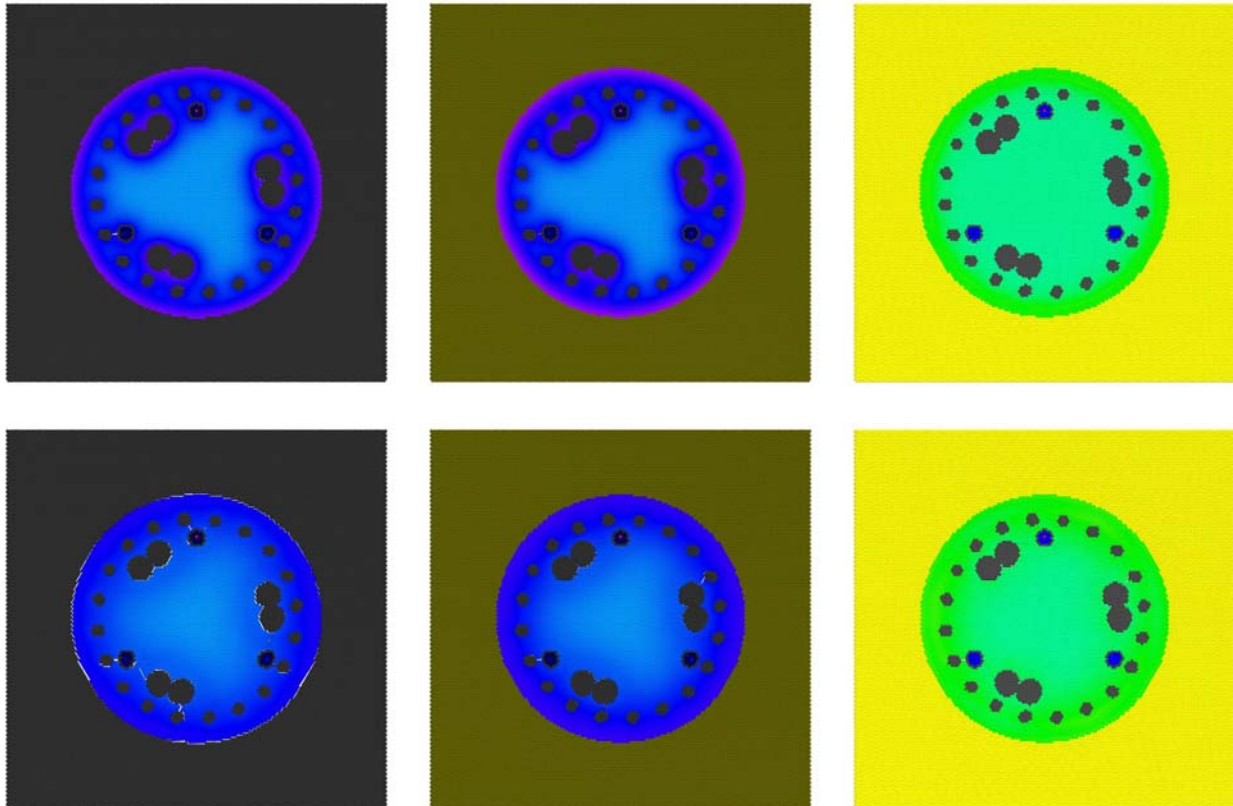


**Figure 5.11. Plot. Curing Heat. Top: 12 hours. Bottom: 24 hours. Left: Rock. Middle: Clay. Right: Difference**

The top row of Figure 5.12 shows heat generation at 2 days. The center of the shaft has fully cured, and has stopped generating additional heat. The concrete in the rock is slightly more mature than the concrete surrounded by clay, as shown in the difference plot.

The bottom row of Figure 5.12 shows heat generation at 3 days. Almost all the concrete has ceased heat generation, except for a very thin section around the perimeter of the shaft surrounded by clay, as shown in the difference plot.

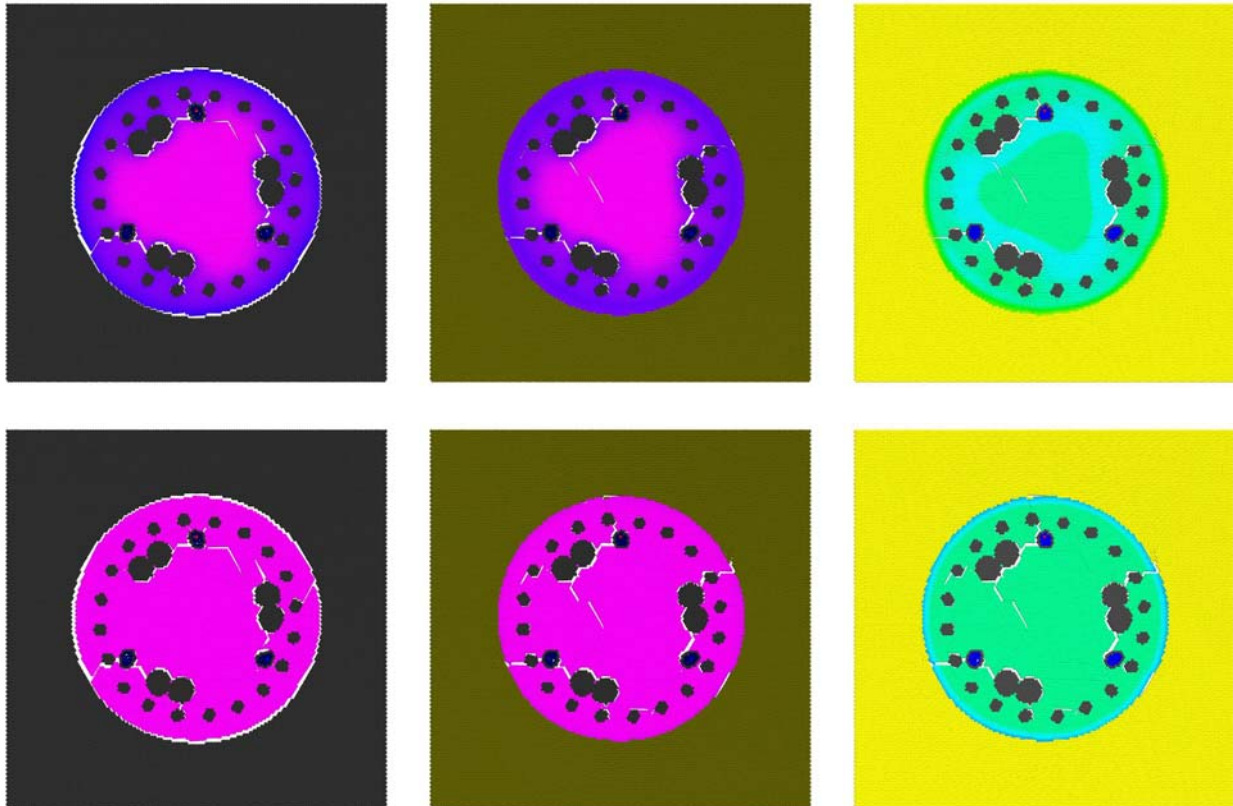


**Figure 5.12. Plot. Curing Heat. Top: 2 days. Bottom: 3 days. Left: Rock. Middle: Clay. Right: Difference**

Figure 5.13 shows that no additional heat is generated after day 4.

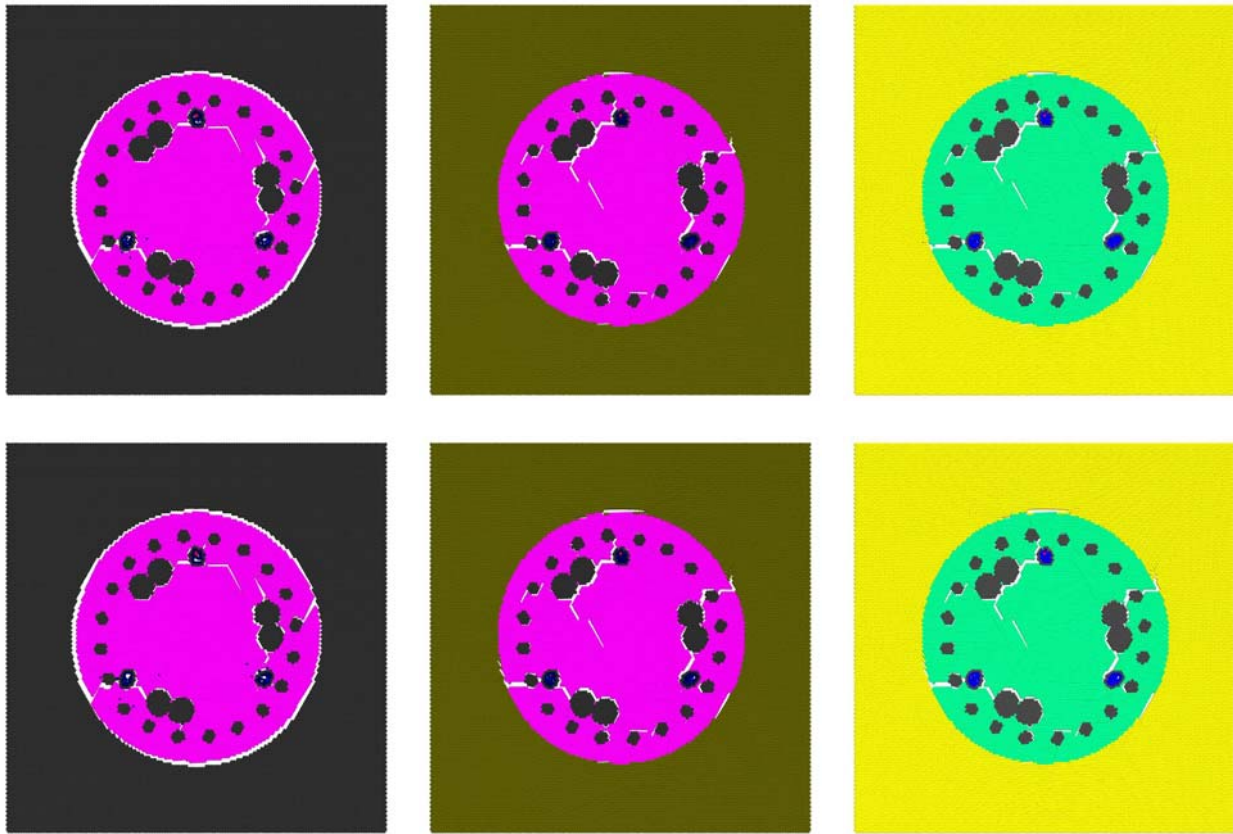


**Figure 5.13. Plot. Curing Heat. Top: 4 days. Bottom: 5 days. Left: Rock. Middle: Clay. Right: Difference**

### 5.3.4 Hydration

The top row of Figure 5.14 shows the hydration phase 4 hours after concrete placement. This is the stage between the first and second hydration phases, and is essentially the same for both drilled shafts. The bottom row of Figure 5.14 shows that the concrete from both shafts begins the second hydration phase at the same time.

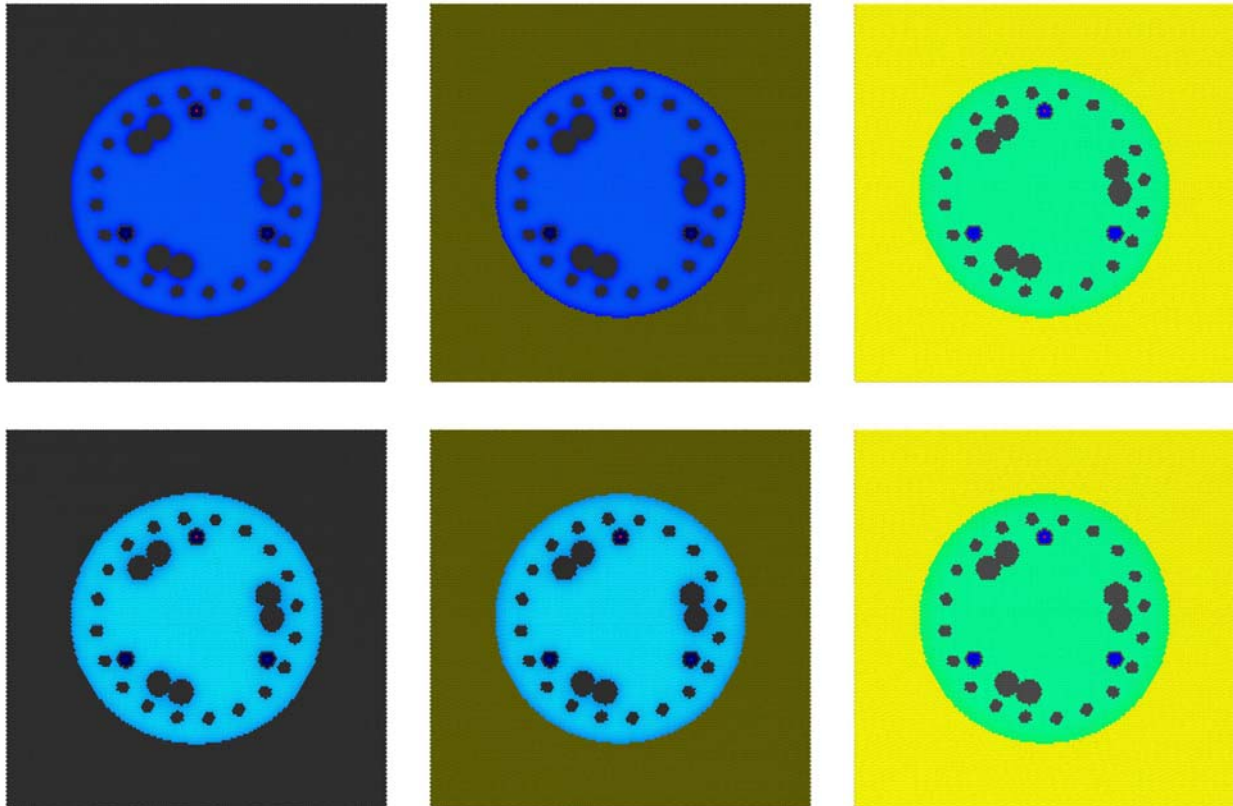


**Figure 5.14. Plot. Curing Hydration. Top: 4 hours. Bottom: 8 hours. Left: Rock. Middle: Clay. Right: Difference.**

Figure 5.15 shows the hydration phase after 12 hours and 24 hours. A more pronounced difference in concrete maturity appears after 24 hours between the inside and outside portions of the shaft, but the surrounding rock and clay have little effect on the hydration phases. Figure 5.16 shows that the center of the shaft reaches maturity before the perimeter, and then stabilizes, as shown in Figure 5.17. Material stiffness, strength, thermal conductivity, and expansion volume follow a similar pattern.

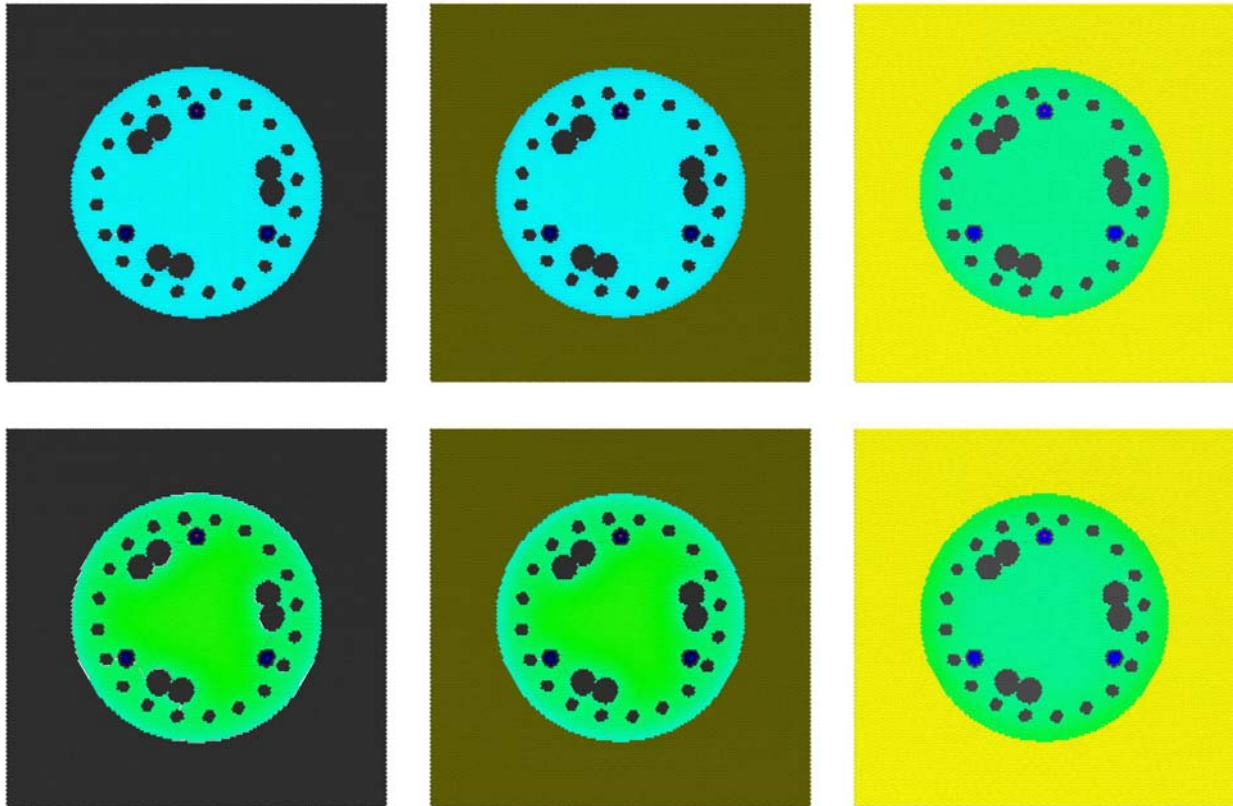


**Figure 5.15. Plot. Curing Hydration. Top: 12 hours. Bottom: 24 hours. Left: Rock. Middle: Clay. Right: Difference**

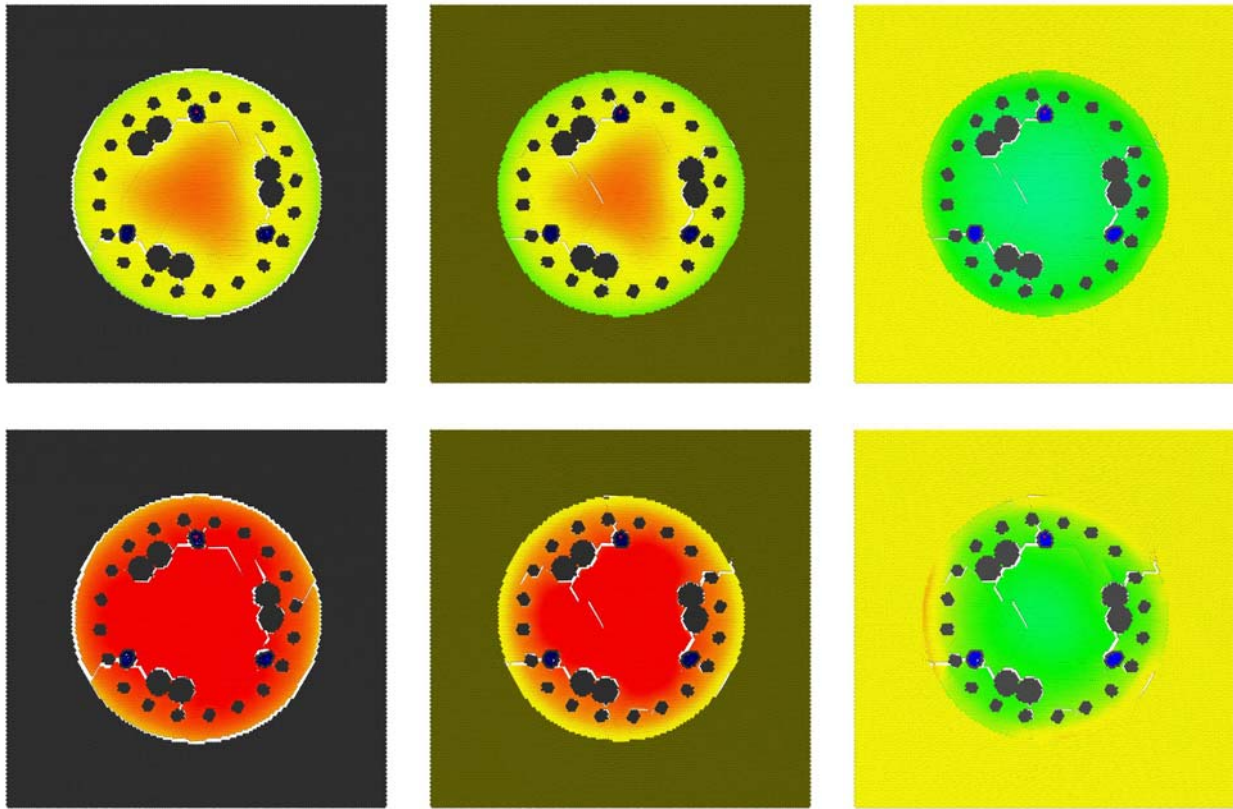


**Figure 5.16. Plot. Curing Hydration. Top: 2 days. Bottom: 3 days. Left: Rock. Middle: Clay. Right: Difference**

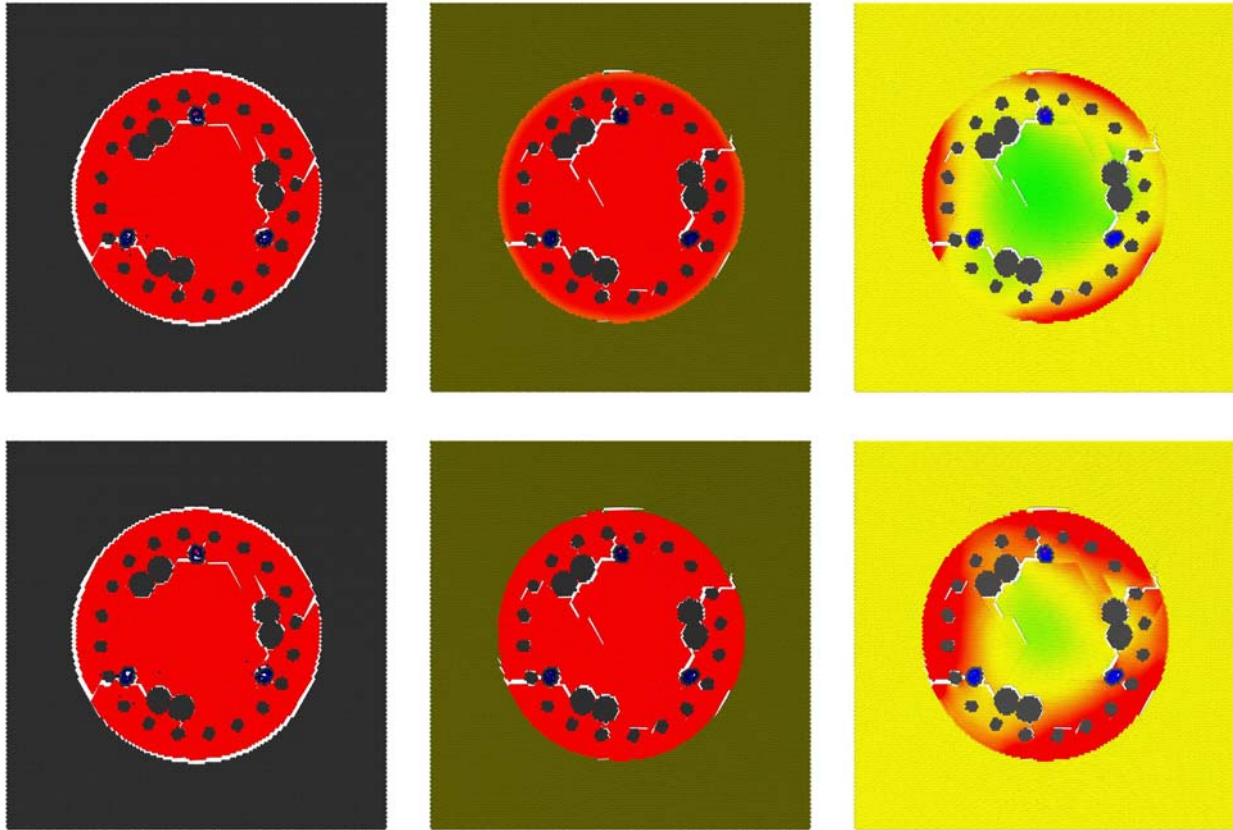


**Figure 5.17. Plot. Curing Hydration. Top: 4 days. Bottom: 5 days. Left: Rock. Middle: Clay. Right: Difference**

### 5.3.5 Temperature

The top row of Figure 5.18 shows the temperature after 4 hours. At this stage, the first hydration phase has completed, and the second hydration phase is in a very early stage. The temperature of the shaft remains high due to the high placement temperature. The temperature is lower in regions around the rebar and access tubes, as heat readily transfers from the warmer concrete to the cooler steel. The halo around the perimeter of difference plot indicates that the temperature of the rock adjacent to the concrete is higher than the temperature of the clay at this location. The temperature of the concrete adjacent to the rock is also at a higher temperature, due to the lower thermal conductivity of the rock. Even though the rock is at a higher temperature, the total amount of heat transferred into the clay is higher, distributed over a larger volume.

The bottom row of Figure 5.18 shows the temperature after 8 hours, when the second hydration phase is beginning to generate heat in warmer regions of the concrete. The temperature becomes more uniform in the perimeter of the shaft, in the region of the rebar cage.

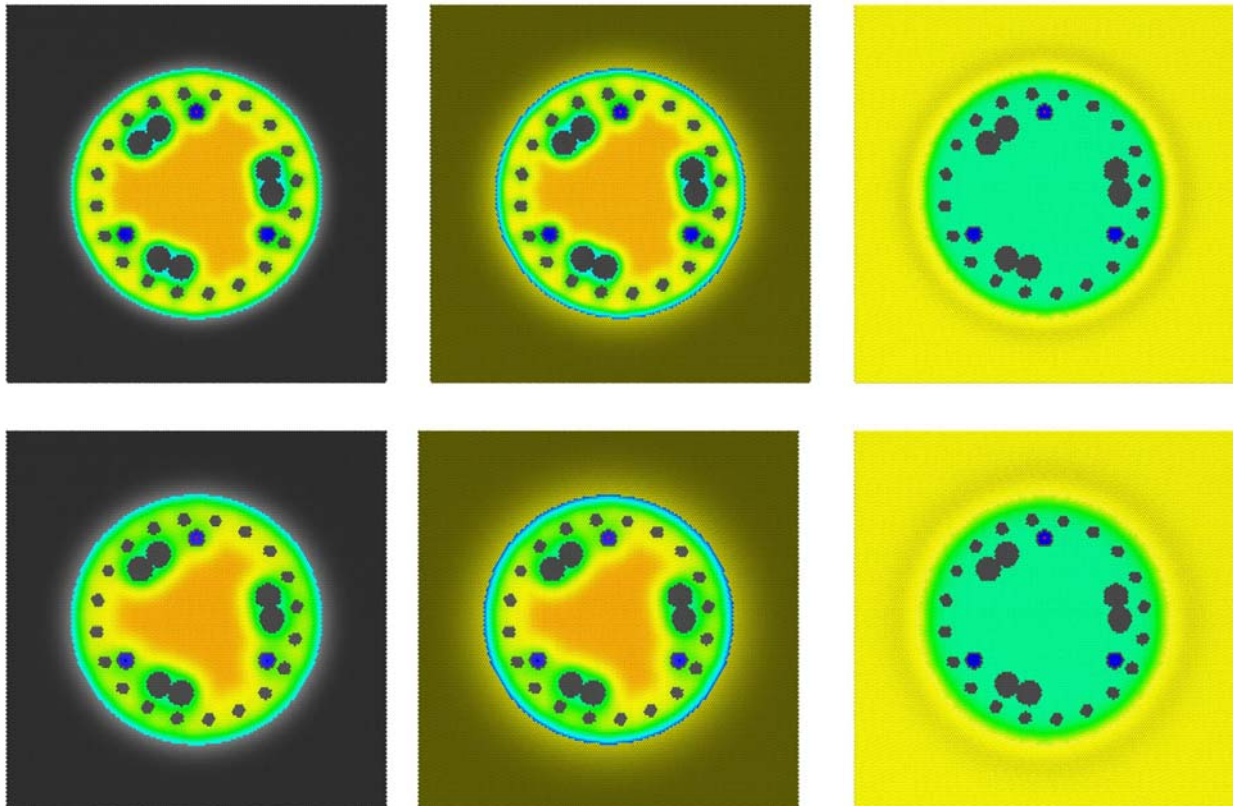


**Figure 5.18. Plot. Curing Temperature. Top: 4 hours. Bottom: 8 hours. Left: Rock. Middle: Clay. Right: Difference**

The top row of Figure 5.19 shows the temperature at 12 hours, as more heat is generated from the second hydration phase. The temperature of the shaft remains high in the center, but decreases around the perimeter, as heat transfers into the surrounding ground. The temperature continues to rise in a larger volume of clay than in the rock. The bottom row shows that the temperature after 24 hours continues to cool around the perimeter of the shaft, and converge to a more stable temperature gradient.

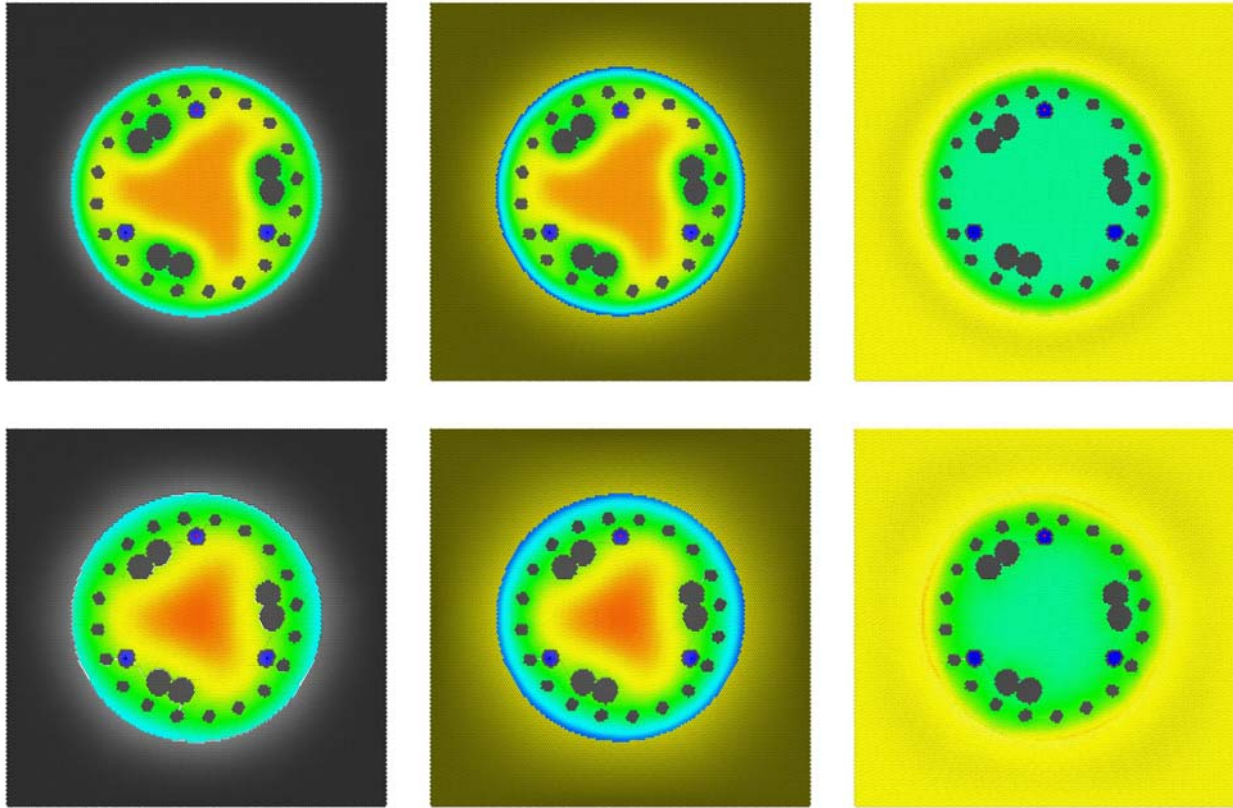


**Figure 5.19. Plot. Curing Temperature. Top: 12 hours. Bottom: 24 hours. Left: Rock. Middle: Clay. Right: Difference**

The top row of Figure 5.20 shows the temperature at 2 days, at the peak of the third hydration phase. Debonding of the rock and concrete results in slight variations in the temperature distribution. Less heat is dissipated by convection, resulting in a significantly higher temperature in the shaft surrounded by rock, especially in the perimeter of the shaft, as shown in the difference figure.

The bottom row of Figure 5.20 shows the temperature at 3 days, at the end of the third hydration phase. The shaft surrounded by rock remains hot, but has a lower temperature gradient as the temperature distributes more evenly throughout the shaft. The temperature around the perimeter of the shaft surrounded by clay is significantly lower, causing a higher temperature gradient in the shaft.

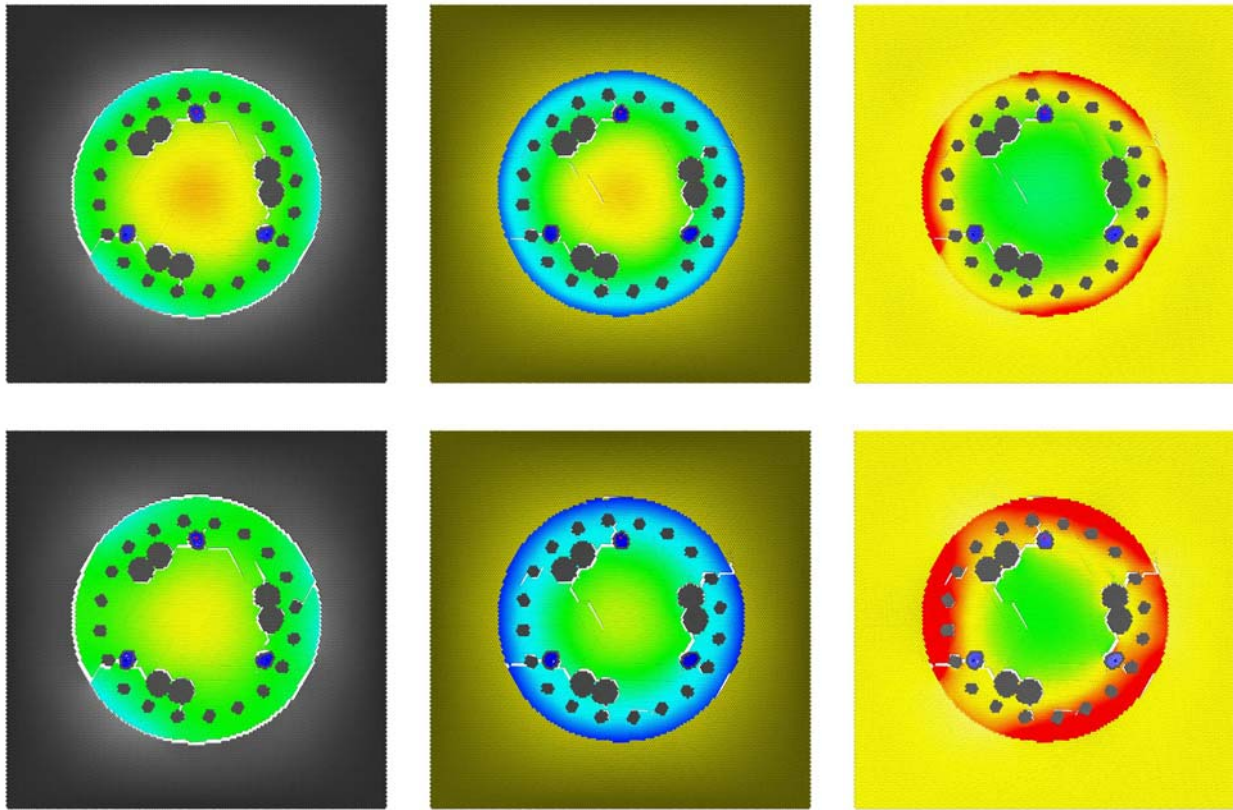


**Figure 5.20. Plot. Curing Temperature. Top: 2 days. Bottom: 3 days. Left: Rock. Middle: Clay. Right: Difference**

After 4 days, the shaft temperature continues to decrease, as shown in Figure 5.21. Much less heat transfers by convection, so the shaft surrounded by rock remains uniformly warm. The core of the shaft surrounded by clay remains warm, and will also require significantly more time to completely cool. The difference plot shows that cracking patterns have a slight effect on temperature.

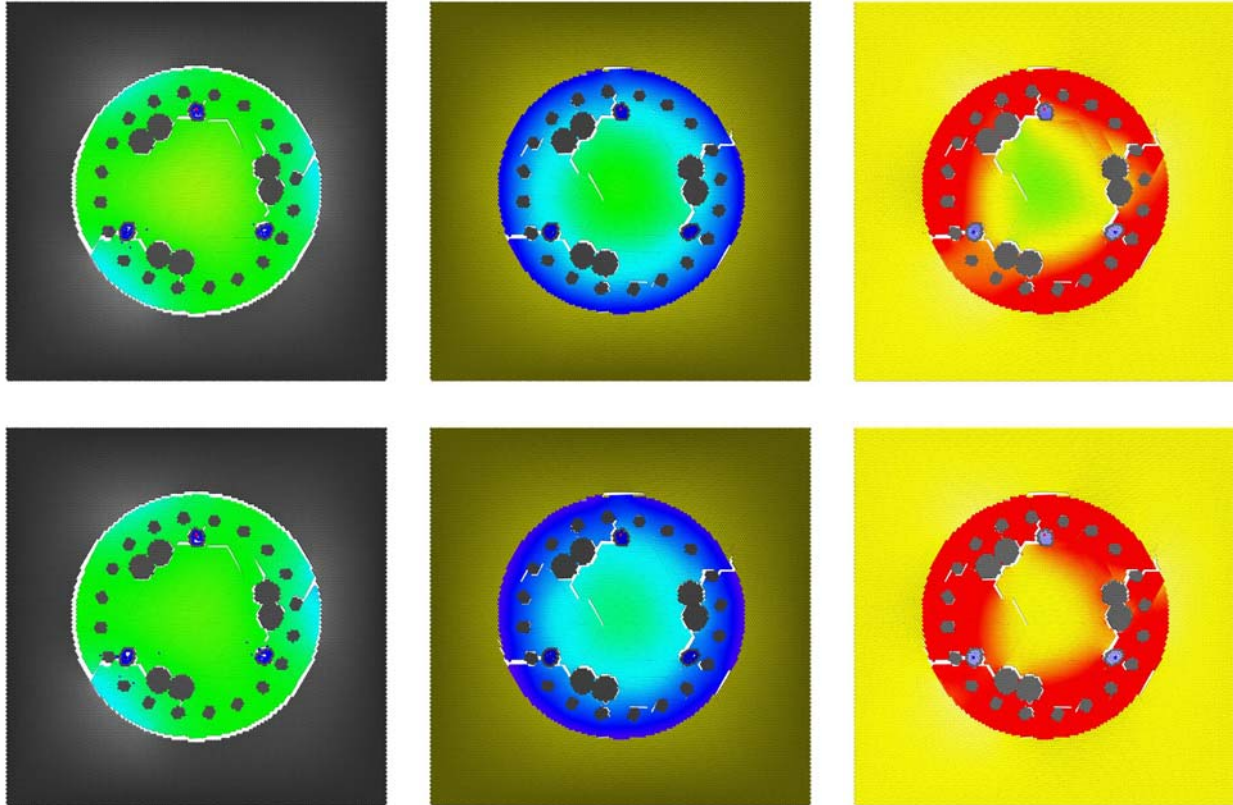


**Figure 5.21. Plot. Curing Temperature. Top: 4 days. Bottom: 5 days. Left: Rock. Middle: Clay. Right: Difference**

## 5.4 Discussion

Internal cracking between rebar is common, and likely occurs in most, if not all, drilled shafts. This is the primary reason why access tubes are placed inside the rebar cage, rather than outside. Tubes placed outside the cage allow more concrete in the shaft to be imaged for defects. CSL data from tubes outside the shaft show very high variability in arrival times and energies. This is commonly attributed to scattering by the rebar and higher signal attenuation from larger tube separation. However, these models show that the variability is actually caused by internal cracking between rebar in the rebar cage, and debonding cracks around the perimeter of the rebar. Sonic compression waves have no problem propagating through rebar and intact concrete. Also, CSL data along the perimeter of the shaft is often ignored, “corrected”, or intentionally not collected on larger shafts with more access tubes, supposedly to save time and cost. CSL velocities are almost always lower along the perimeter of the shaft than through the center, even when tubes are placed inside the rebar cage. This is often attributed to differences in concrete

maturity and lower temperatures in regions along the perimeter. However, these lower velocities persist long after all the concrete in the shaft has fully cured. Since cracking is common in the region of the rebar cage, slower velocities and higher variability will result between tubes along the perimeter.

Cracks develop from the rebar to the outside of the shaft. These cracks are serious concerns for corrosion, because they provide a conduit for corrosives to reach the rebar and deteriorate the shaft. Since cracks initiate at the rebar, any cracks that extend to the outside of the shaft will lead directly to a rebar support. Since cracks extend between rebar in the support cage, more rebar is directly exposed to corrosives from a single external crack than is readily apparent.

As this study indicates, variability and reduction of CSL velocities and energies can result from cracking. Indications of internal cracks from lower velocity CSL surveys are often nerve-racking, and can result in litigation. Ignoring or side-stepping the issue is not an option.